Steady and unsteady aerodynamics

M.F. Platzer & K.D. Jones
AeroHydro Research & Technology Associates, Pebble Beach, CA, USA.

Abstract

This paper discusses the major flow features encountered by conventional airfoils in low-speed flows. To this end, steady flow over a NACA 0012 airfoil at zero, moderate, and near-stall incidence angles is described. This is followed by a discussion of the unsteady flow phenomena caused by sudden changes in airfoil incidence angle or by airfoil oscillation.

1 Introduction

In the first paper of this volume [1] the fundamentals of lift and drag generation were presented and it was shown that lift is linked to vortex generation and drag is critically dependent on the state of the flow (i.e. attached or separated) and on the state of the boundary layer (i.e. laminar or turbulent). It is instructive to study the changes in flow features in response to various parameter changes, such as changes in incidence angle and Reynolds number. To keep the discussion in bounds, we limit ourselves to two-dimensional incompressible flows, i.e. to low-speed airfoil flows. To this end, we consider only one representative airfoil shape and choose the NACA 0012 airfoil. Nevertheless, even with this restriction, very different flow phenomena are obtained. One has to distinguish between attached flow at zero or moderate incidence angle, flow close to and beyond flow separation, flow due to rapid incidence change without flow separation, flow due to rapid incidence change with flow separation and flow due to airfoil oscillation. All these flows are dependent on the chosen Reynolds number. These cases are therefore discussed separately in the following sections.

2 Steady low-speed airfoil flow at zero or moderate incidence angle

In Fig. 1 we show the pressure, boundary layer thickness and skin friction distributions caused by an incompressible flow of Reynolds number 1 million over the NACA 0012 airfoil at zero incidence angle. The pressures are indicated as pressure differences relative to the free-stream pressure and are made nondimensional by dividing them by the free-stream dynamic pressure.

WIT Transactions on State of the Art in Science and Engineering, Vol 4, © 2006 WIT Press
www.witpress.com, ISSN 1755-8336 (on-line)
doi:10.2495/1-84564-095-0/6a

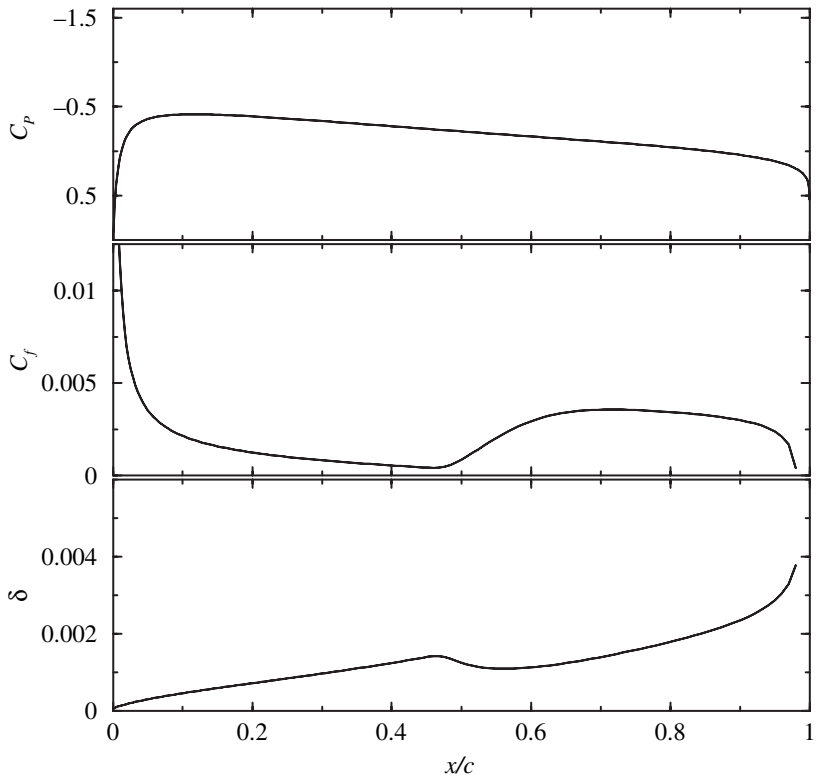

Figure 1: Pressure, skin friction and boundary layer thickness on the NACA 0012 airfoil at zero incidence angle, Reynolds number = 1 million [3].

The boundary layer thickness is given as a percentage of the airfoil chord length. The skin friction is also made nondimensional by dividing it by the free-stream dynamic pressure. The NACA 0012 airfoil being a symmetrical airfoil the flow in the upper and lower half-planes is symmetrical and therefore the pressure distributions on the upper and lower airfoil surfaces are the same. The speed of the fluid particles near the airfoil has to increase so that the particles can get past the airfoil and therefore, according to the Bernoulli law, the pressures decrease below the free-stream pressure over most of the airfoil surface except near the stagnation point at the rounded nose. This can be seen in Fig. 1 (top) where the pressures are displayed in the form of pressure coefficients. A negative value implies a pressure below the free-stream pressure and hence, according to the Bernoulli law, a velocity greater than the free-stream speed. As already explained in the first paper of this volume, inviscid potential flow theory is quite useful in analyzing this flow problem. But, as also pointed out, an inviscid flow solution will predict zero drag because the pressure will rise again to the stagnation pressure at the trailing edge, thereby counterbalancing the overpressures near the nose. The inability of potential flow solutions to predict drag is referred to in the literature as d'Alembert's paradox. In a viscous flow the fluid particles are decelerated to zero relative speed at the airfoil surface (no-slip condition) and a viscous boundary layer starts to build up starting from the stagnation point at the airfoil nose becoming thicker with increasing distance from the nose. Prandtl recognized that the thickness of this boundary layer remains quite small for

flows of sufficiently large Reynolds number. In most aeronautical engineering applications the Reynolds number (based on the airfoil chord) is at least several hundred thousand or, more often, several million. In such cases Prandtl's approach [2] to split the analysis into two steps works quite well, i.e. obtain the pressure distribution by means of a potential flow analysis because the pressure changes very little within the boundary layer at a given airfoil station and then perform the boundary layer analysis using the previously determined pressure distribution as input. The results obtained by such an approach, using the computer programs documented in reference [3], are shown in Fig. 1 (middle), where the skin friction is plotted, and in Fig. 1 (bottom), where the boundary layer thickness distribution is shown. The boundary layer flow starts out as a laminar flow near the nose because the flow velocities are small. It remains laminar as long as the flow is accelerating, i.e. as long as the pressures are falling. However, the flow in the boundary layer becomes turbulent soon after the fluid particles enter a region of increasing (i.e. adverse) pressure gradient and finally the flow starts to separate very near the trailing edge. As a consequence, a finite drag is generated because of the friction effect caused by the laminar and turbulent boundary layers (skin friction drag) and because of the separated flow region near the trailing edge (pressure drag). Note that the transition to turbulent flow manifests itself by a marked increase in skin friction and it occurs downstream of the point of maximum airfoil thickness. These predictions are found to agree quite well with measurements of the pressure, boundary layer thickness and skin friction distributions.

In Fig. 2 we show the same information, in addition to the results obtained after setting the airfoil to an incidence angle of 4°. It is immediately evident that the upper surface pressures are significantly lower at 4° than at 0°, especially near the leading edge, whereas the pressures on the lower surface are substantially higher than the zero incidence pressures. Hence suction is generated on the upper surface, with a distinct suction peak near the leading edge. Therefore, the upper surface is often referred to as suction surface and the lower surface as pressure surface. The pressure difference between the pressure and suction surfaces adds up to a finite lift. Note that the largest pressure differences occur over the forward half of the airfoil. Therefore, the resultant lift acts at or near the quarter chord point. The pressures on the lower surface are greater than the free-stream pressure and this airfoil surface is therefore called the pressure surface. As mentioned in the first paper of this volume, Newton hypothesized that the lift is generated by overpressure on the lower surface due to the impact of the fluid particles on the lower surface. However, as can be seen from the pressure distributions shown in Fig. 2, the suction effect on the upper surface contributes more to the resultant lift than the overpressure on the lower surface. The skin frictions and boundary layer thicknesses shown in Fig. 2 (middle and bottom) reveal that on the suction surface the boundary layer transition has moved upstream close to the leading edge because the adverse pressure gradient region starts close to the leading edge. Of particular importance is the fact that the transition to turbulent flow prevents the onset of flow separation near the leading edge. Again, as already mentioned in the first paper of this volume, a laminar boundary layer is much less resistant to flow separation than a turbulent one. This fact manifests itself by the behavior of the laminar skin friction. It is seen that the laminar skin friction drops rapidly toward a zero value, which is indicative of the onset of flow separation. Fortunately, the flow becomes turbulent before then and the onset of airfoil stall is prevented. As in the case of laminar versus turbulent flow over the sphere, discussed in the first paper of this volume, the transition to turbulent flow is quite beneficial in this case. As a matter of fact, flight at lower Reynolds numbers is much trickier because there is a greater tendency toward flow separation. These phenomena have become of increasing interest and importance with the development of small unmanned air vehicles and especially of micro air vehicles.

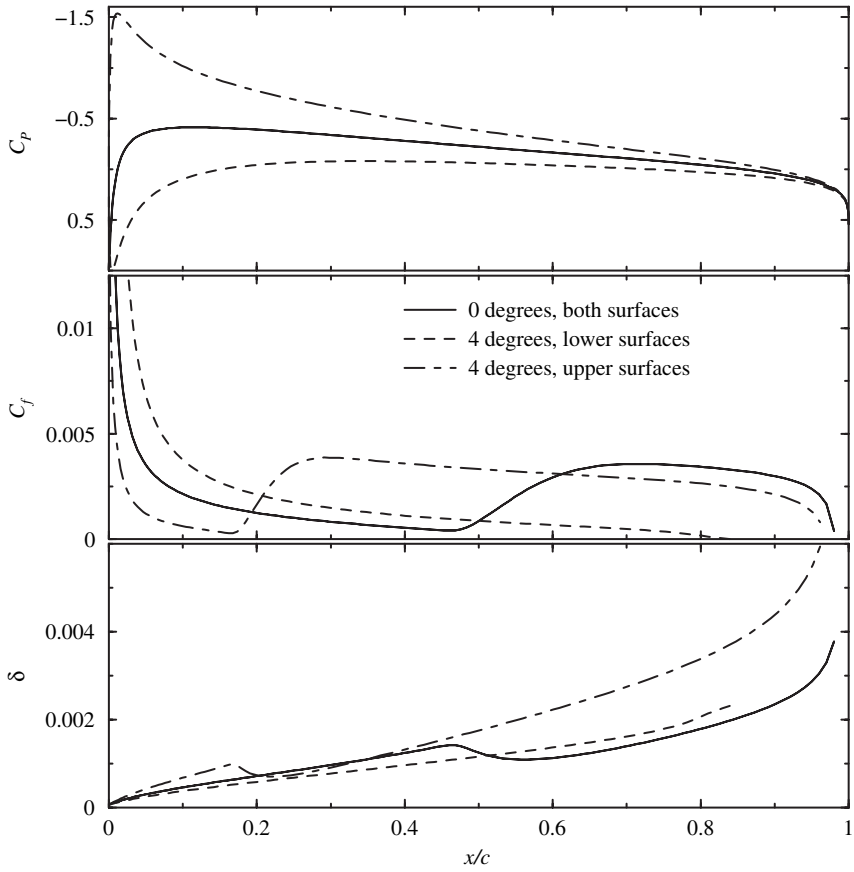

Figure 2: Comparison of the aerodynamic characteristics of the NACA 0012 airfoil at 0° and 4° incidence angle, Reynolds number = 1 million [3].

3 Low-speed airfoil flow near the stall angle

A further increase of the incidence angle inevitably leads to the onset of flow separation which is initially limited to a small region near the leading edge where the fluid particles first encounter an adverse pressure gradient. The fluid particles reverse flow direction only to be swept downstream again by the neighboring particles farther away from the airfoil surface. As a consequence, a so-called leading-edge separation bubble is formed near the leading edge which contains recirculatory flow. A bubble of this type is shown in Fig. 3, based on an interferogram taken by M.S. Chandrasekhara [4], visualizing the flow over a NACA 0012 airfoil at an incidence angle of 10° in a flow of Reynolds number 540,000.

A progressive increase in the incidence enlarges the separation bubble until the flow breaks away quite massively at an incidence angle of 11.95°, as shown in Fig. 4. This is the condition of airfoil stall. The suction that contributed the major part of the lift at the lower incidence angles cannot be maintained any longer, causing a large loss in lift. This is shown in Fig. 5 for the NACA 0012 airfoil, taken from reference [5] which contains measured lift and pitching moment coefficient (about the quarter-chord point) data on many airfoils. Note the effect of Reynolds number.

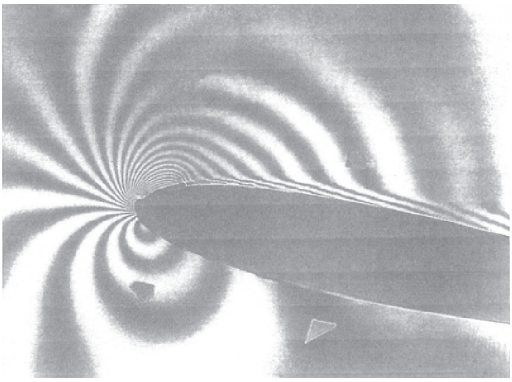

Figure 3: Development of a leading-edge separation bubble [4].

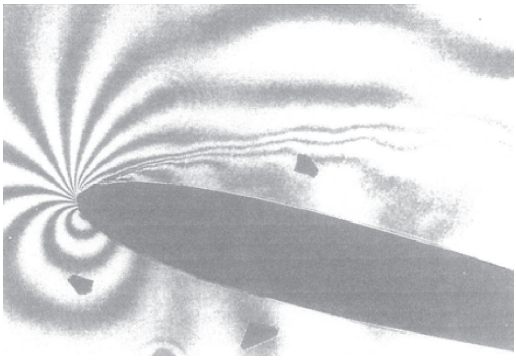

Figure 4: Leading-edge stall on the NACA 0012 airfoil [4].

The stall angle increases with increasing Reynolds number. Also note that the inviscid flow theory (solid line) cannot predict the onset of stall. Furthermore, it is also important to note that the flow ceases to remain steady as soon as the stall angle is exceeded. The large wake flow generated by the flow separation near the leading edge becomes a fluctuating three-dimensional flow.

The onset of stall and the resulting loss of lift depend on the airfoil geometry. Thin airfoils tend to generate leading-edge stall of the type described above for the NACA 0012 airfoil. On the other hand, on thick airfoils the flow separation typically starts from the trailing edge. As a result, the loss in lift is much more benign. Readers interested in further details can refer to the work by Abbott and von Doenhoff [5] and Eppler [6].

4 The Wagner effect

As already pointed out in the first paper of this volume, the physics of lift generation becomes much more understandable by considering the vortex shedding process from the airfoil's trailing edge in response to a sudden incidence change. Herbert Wagner [7] was the first to provide a mathematical solution to this problem in 1925. Using the linearized inviscid incompressible flow theory he derived the lift response plotted in Fig. 6. It shows that the lift builds up only gradually to the steady-state value after a sudden small change in the incidence angle. A closer inspection of

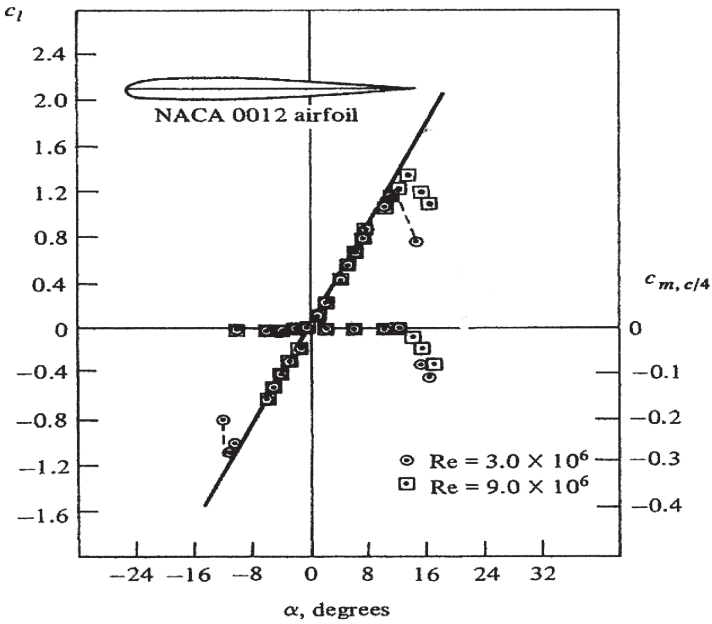

Figure 5: Lift and pitching moment of the NACA 0012 airfoil as a function of the incidence angle [5].

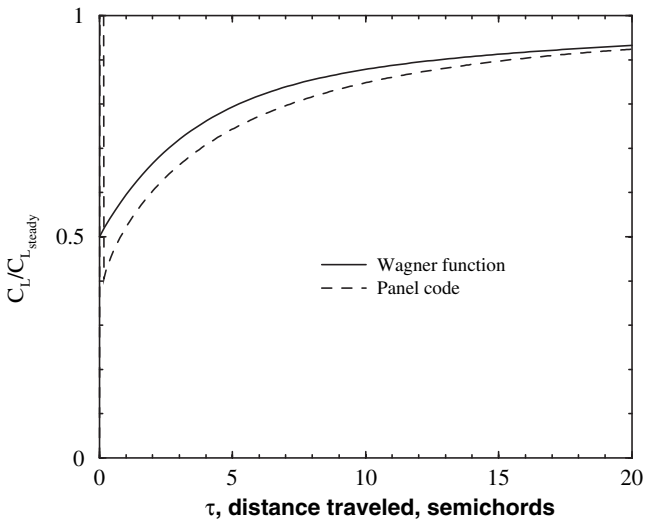

Figure 6: Lift response due to sudden incidence change [7].

his solution reveals that the lift is infinitely large immediately after the incidence change, but drops immediately to half the steady-state value and then increases gradually to the steady-state value. The very large lift value immediately after the incidence change is caused by the incompressible flow assumption causing the air to be completely 'unyielding' in the first instant after the incidence change. The gradual growth to the lift value corresponding to the new incidence angle, on the

other hand, is caused by the shedding of the starting vortex. This counterclockwise vortex has a strong influence on the velocity and pressure field around the airfoil as long as it remains in close proximity. As can be seen from Fig. 6, the airfoil travels about 20 half-chord lengths until the lift reaches about 95% of the final value. Another way of explaining the Wagner effect is to say that it is caused by the fluid's 'memory'. Vortices shed at an earlier time are being 'remembered' because they are being carried downstream only with a finite velocity. Wagner obtained his solution for an infinitely thin flat plate. The panel code solution differs somewhat from this solution because it is obtained for a finite thickness airfoil.

5 The Kramer effect

In 1932 Max Kramer [8] performed wind tunnel experiments that were stimulated by the observations of some pilots that 'gusty air was better than calm air' as far as lift was concerned. Rapid changes in the incidence angle appeared to generate inexplicably high lift values, in clear contradiction to the Wagner effect. He therefore conceived an experiment which allowed him to simulate a sudden vertical gust in the wind tunnel and which confirmed the pilot observations. Rapid incidence angle changes produced lift values that exceeded the corresponding steady-state values. The effect was measured to be directly proportional to the rate of incidence angle change. Kramer postulated that the most probable explanation for this effect was the inertia of the flow separation process.

In the ensuing years this dynamic lift or stall effect has been studied in considerable detail, both experimentally and computationally, because of its importance in the operation of flight vehicles and wind turbines. For example, helicopter blades may fail due to exposure to dynamic stall. On the other hand, fighter aircraft designers have tried to take advantage of dynamic lift to improve fighter maneuverability.

The fundamental difference between the static and dynamic airfoil stall phenomena is shown in Fig. 7 which is based on low-speed wind tunnel measurements by Carr *et al.* [9]. As already found by Kramer, an airfoil that is pitched rapidly through the static stall angle produces a lift much greater than the maximum observed at a steady angle of attack. Due to the delay in pressure buildup, similar to the delay responsible for the Wagner effect, the boundary layer separation is delayed on the suction surface and the lift continues to increase past the maximum static lift. Eventually, flow reversal occurs in the boundary layer which is followed by the development of a clockwise vortex near the leading edge. This vortex keeps growing and moving over the upper airfoil surface, thereby inducing low pressures on this surface. As a result, a substantially larger pressure difference between the lower and upper surfaces, and therefore a larger lift, is induced than would be possible under static conditions. Therefore, for a short period of time lift values that can be twice the static values are produced. However, this beneficial effect is lost as soon as the dynamic stall vortex approaches the trailing edge. As seen in Fig. 7, the lift decreases abruptly while, at the same time, a sharp pitching moment spike is induced. As the airfoil incidence is reduced, the fully stalled flow over the suction surface starts to reattach. Hence the flow behavior during the pitch-up and pitch-down strokes is quite different, leading to the hysteresis loops shown in Fig. 7. This is further illustrated in Fig. 8 showing the suction surface pressure distributions measured by McAlister *et al.* [10] on a NACA 0012 airfoil which is oscillated with an amplitude of 10° around a fixed angle of 15°. Note the very large suction peaks near the leading edge followed by an abrupt collapse of the leading edge suction.

These dynamic stall features can vary significantly, depending on airfoil shape, free-stream Reynolds number and Mach number, and flow three-dimensionality. The prediction of dynamic

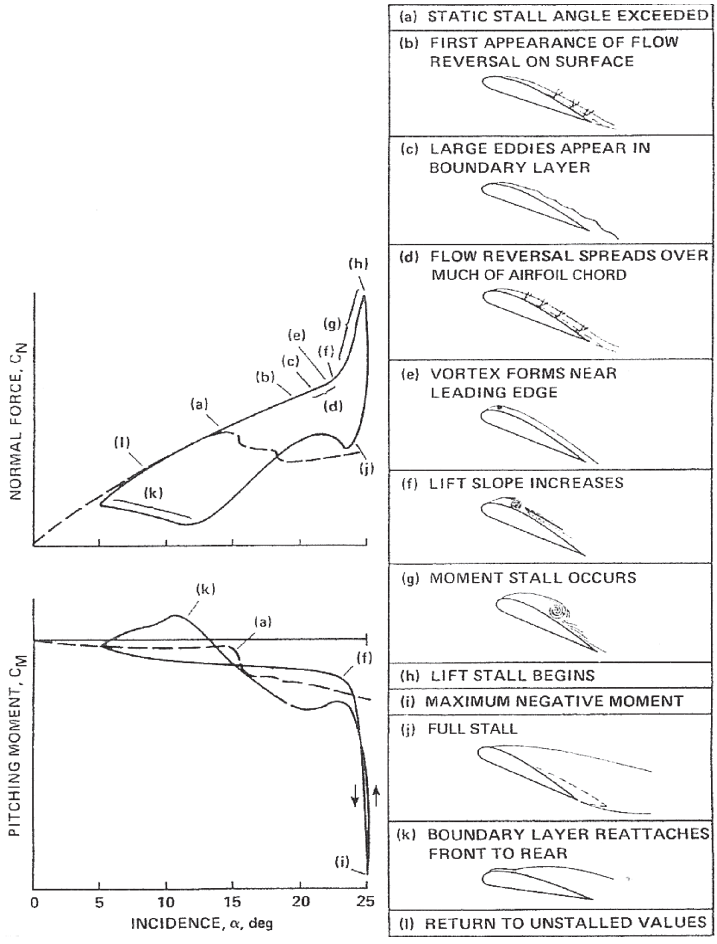

Figure 7: Dynamic airfoil stall [9].

stall has advanced considerably in recent years with the development of two- and three-dimensional Navier–Stokes codes, but there are a number of flow phenomena that still defy currently available computational methods, such as the prediction of the effect of transition from laminar to turbulent flow, the prediction of flow reattachment, etc. For recent reviews of the physics and prediction of dynamic stall we refer the reader to references [11, 12].

6 The Katzmayr effect

Birds, insects, fish and mammals have used flapping-wing propulsion for millions of years. Early flight pioneers, such as O. Lilienthal in the 1890s, were fascinated by the birds' ability to fly by flapping their wings, yet attempts to build flapping-wing flight vehicles were soon abandoned in favor of fixed-wing or rotary-wing aircraft. Nevertheless, the physics of thrust generation due to wing flapping was unraveled at about the same time as the physics of lift generation. Knoller [13] in 1909 and Betz [14] in 1912 noted that a flapping wing encounters an induced angle of attack, which cants the aerodynamic force vector forward such that it has a lift and a thrust force component.

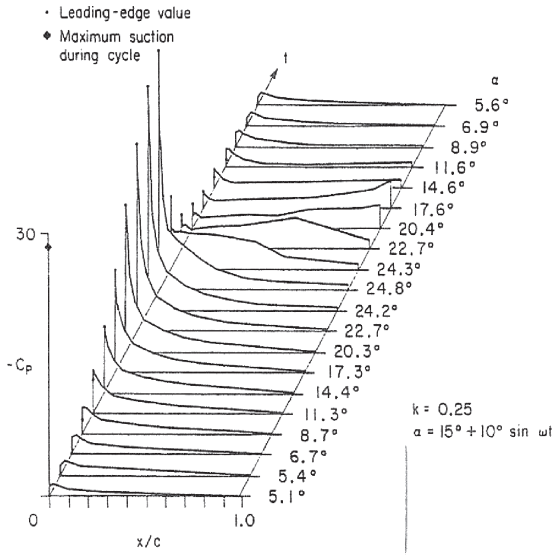

Figure 8: Upper surface pressure changes due to dynamic stall [10].

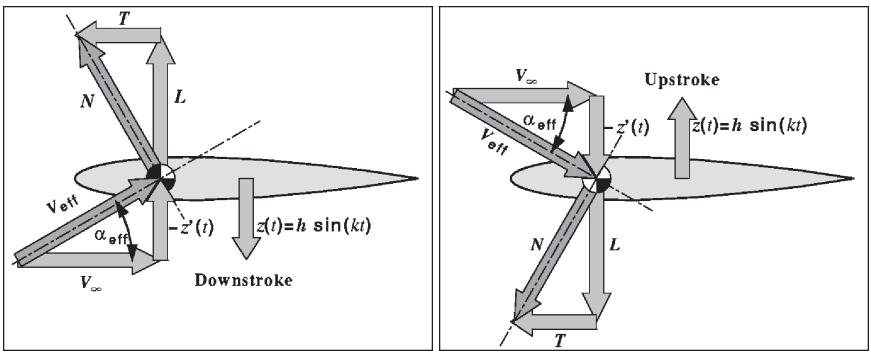

Figure 9: Basic principle of thrust generation due to airfoil flapping.

The basic principle is illustrated in Fig. 9, where the airfoil is shown during the downstroke in the image on the left and in the upstroke in the image on the right. The harmonic flapping motion produces an induced velocity such that the effective velocity is at an angle with respect to the chordline. The resultant aerodynamic force vector (neglecting viscous effects) is then normal to the velocity seen by the airfoil, and is therefore canted forward, yielding a sinusoidally varying thrust whose time average is a net thrust. This Knoller–Betz elementary theory does not include the effect of the starting vortices which must be shed at the trailing edge due to the continuous incidence angle change of the airfoil. Its inclusion was first achieved by von Karman and Burgers [15] in 1935 who offered the first explanation of thrust production based on the observed location and orientation of the wake vortices shown in Fig. 10.

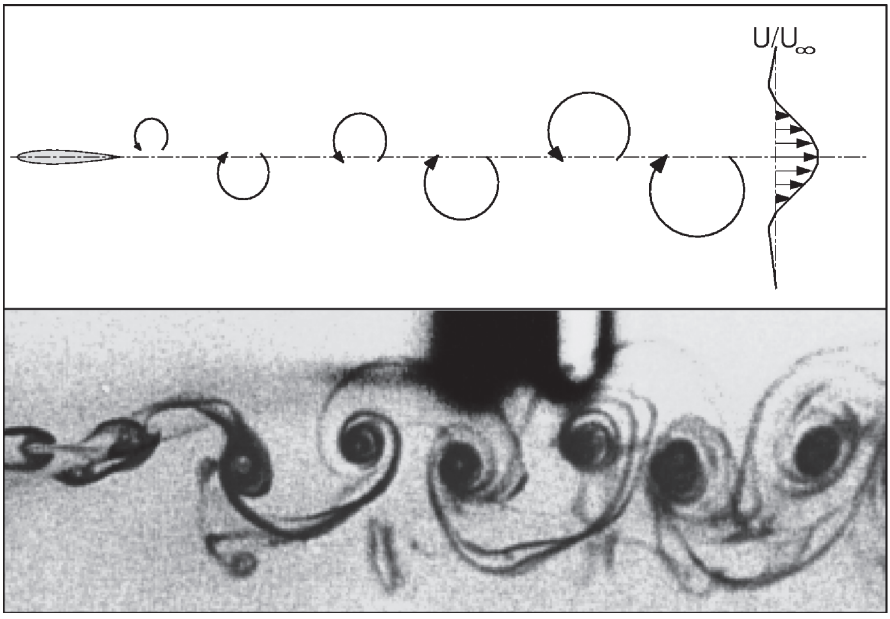

Figure 10: Vortex street behind a harmonically plunging airfoil [16].

However, in 1922, Katzmayr [17] had already provided the first experimental verification of the Knoller–Betz theory. He chose to oscillate the flow rather than the airfoil, recognizing the approximate equivalence of both arrangements. His measurements indeed yielded a net thrust acting on the airfoil.

The basic physics of the thrust generation due to airfoil flapping becomes clear by looking at Fig. 10. The largest changes in positive or negative incidence angle occur when the airfoil moves through the top or bottom positions, respectively. Therefore, during one cycle the airfoil sheds counterclockwise vorticity as it passes through the top position, followed by clockwise vorticity as it passes through the bottom position. As a result, a vortex street is being generated downstream of the airfoil, which induces a velocity increase between the two rows. The sinusoidally plunging airfoil therefore acts like a conventional propeller that captures a certain amount of fluid and gives it an increased time-averaged velocity. Measurements of the time-averaged velocity downstream of the trailing edge indeed yield a jet-like velocity profile [18]. Hence the flapping airfoil becomes a 'jet engine' that propels the bird forward by ejecting a certain amount of fluid in the opposite direction.

References

[1] Platzer, M.F. & Jones, K.D., Concepts of aero- and hydromechanics. *Flow Phenomena in Nature*, Vol. 1, pp. 5–19, 2006.

[2] Prandtl, L., Ueber Fluessigkeitsbewegung bei sehr kleiner Reibung. *Verhandlungen des III Internat. Math. Kongr.*, Heidelberg, 8–13 August 1904, Teubner: Leipzig, pp. 484–491, 1905.

[3] Cebeci, T., Platzer, M.F., Chen, H., Chang, K.C. & Shao, J.P., *Analysis of Low-Speed Unsteady Airfoil Flows*, Springer: Berlin, 2005.

[4] Carr, L.W., Chandrasekhara, M.S. & Brock, N., A quantitative study of unsteady compressible flow on an oscillating airfoil. *Journal of Aircraft*, **31(4)**, pp. 892–898, 1994.
[5] Abbott, I.H. & von Doenhoff, A.E., *Theory of Wing Sections*, Dover Publications: New York, 1959.
[6] Eppler, R., *Airfoil Design and Data*, Springer-Verlag: Berlin, Heidelberg, New York, 1990.
[7] Wagner, H., Ueber die Entstehung des dynamischen Auftriebes von Tragfluegeln. *Zeitschrift für Angewandte Mathematik und Mechanik*, **5(1)**, 1925.
[8] Kramer, M., Die Zunahme des Maximalauftriebes von Tragfluegeln bei ploetzlicher Anstellwinkelvergroesserung. *Zeitschrift für Flugtechnik und Motorluftschiffahrt*, **23(7)**, pp. 185–189, 1932.
[9] Carr, L.W., McAlister, K.W. & McCroskey, W.J., Analysis of the development of dynamic stall based on oscillating airfoil experiments, NAS TN D-8382, 1977.
[10] McAlister, K.W., Carr, L.W. & McCroskey, W.J., Dynamic stall experiments on the NACA 0012 airfoil, NASA TP-1100, 1978.
[11] Ekaterinaris, J.A., Chandrasekhara, M.S. & Platzer, M.F., Recent developments in dynamic stall measurements, computations and control, AIAA Paper No. 2005-1296, January 2005.
[12] Ekaterinaris, J.A. & Platzer, M.F., Computational prediction of airfoil dynamic stall. *Progress in Aerospace Science*, **33**, pp. 759–846, 1997.
[13] Knoller, R., Die Gesetze des Luftwiderstandes. *Flug- und Motortechnik (Wien)*, **3(21)**, pp. 1–7, 1909.
[14] Betz, A., Ein Beitrag zur Erklaerung des Segelfluges. *Zeitschrift fuer Flugtechnik und Motorluftschiffahrt*, **3**, pp. 269–272, 1912.
[15] von Karman, T. & Burgers, J.M., General aerodynamic theory—perfect fluids. *Aerodynamic Theory*, Vol. II, ed. W.F. Durand, Julius Springer: Berlin, p. 308, 1934.
[16] Jones, K.D., Lund, T.C. & Platzer, M.F., Experimental and computational investigation of flapping wing propulsion for micro air vehicles (Chapter 16). *Progress in Astronautics and Aeronautics*, Vol. 195, American Institute of Aeronautics and Astronautics, 2001.
[17] Katzmayr, R., Effect of periodic changes of angle of attack on behavior of airfoils. NACA TM 147, October 1922.
[18] Lai, J.C.S. & Platzer, M.F., Jet characteristics of a plunging airfoil. *AIAA Journal*, **37(12)**, pp. 1529–1537, 1999.